PCT/AU2004/001338

PRIORITY DOCUMENT
SUBMITTED OR TRANSMITTED IN COMPLIANCE WITH RULE 17.1(a) OR (b)

Patent Office
Canberra

I, JULIE BILLINGSLEY, TEAM LEADER EXAMINATION SUPPORT AND SALES hereby certify that annexed is a true copy of the Provisional specification in connection with Application No. 2004900214 for a patent by COMMONWEALTH SCIENTIFIC AND INDUSTRIAL RESEARCH ORGANISATION as filed on 16 January 2004.

WITNESS my hand this
Thirteenth day of October 2004

J. Billingsley

JULIE BILLINGSLEY
TEAM LEADER EXAMINATION
SUPPORT AND SALES

AUSTRALIA

Patents Act 1990

PROVISIONAL SPECIFICATION

Applicant:

COMMONWEALTH SCIENTIFIC AND INDUSTRIAL RESEARCH ORGANISATION

Invention Title:

AN INFRARED DETECTION APPARATUS

The invention is described in the following statement:

Title

AN INFRARED DETECTION APPARATUS

Field of the Invention

The present invention relates to an infrared detection apparatus for monitoring a field of view in order to detect an adverse atmospheric condition. The apparatus has particular application to detecting sulphur dioxide, volcanic ash and wind-blown dust.

Background to the Invention

There are a number of adverse atmospheric conditions which it would be desirable to detect. These include volcanic ash, toxic gases such as sulphur dioxide gas and wind-blown dust.

Volcanic ash is a hazard to jet aircraft, causing engines to stall when ingested, scouring windows and the leading edges of the wings and causing instrument malfunctions. Damage to aircraft can be counted in the millions of dollars. Most serious aircraft encounters with ash clouds have been at cruise altitudes, but there is also a hazard to aircraft at airports affected by volcanic ash. These airports are usually close to an active volcano (e.g. Anchorage and Kagoshima) but they can also be at some distance from the source of the eruption due to atmospheric transport that brings ash into the region.

The cost of ash hazards to airport operations is not known, but must be significant if the costs include those due to delays to landings and take-offs as well as re-routing costs incurred by airline operators. Currently there are no regulatory requirements for airport operators to provide warnings of ash hazards. Warnings are issued

based on information from volcano observatories, meteorological advisories and, in some cases, radar observations of eruption columns. Radar information is generally only reliable at the start of an eruption when the ash cloud is thick and usually such information is only available at airports in close proximity to an erupting volcano. For airports distant from the source of ash there are few direct observations available. Some observations come from satellite systems and other sources of information come from trajectory forecasts based on wind data and cloud height information. Much of this information is sporadic and untimely and there is a need for better detection systems.

Other adverse atmospheric conditions include the toxic gases emitted by volcanoes and industrial plants. Of particular importance and abundance is sulphur dioxide gas. This gas is colourless, but has a characteristic pungent odour. Eye irritation and inflammation of the respiratory tract occurs in relatively low concentrations. Amounts of 6-12 ppm will cause immediate irritation of the nose and throat. Long term exposure can exacerbate asthma and can be dangerous to persons with preexisting cardiopulminary diseases. Thus monitoring near to strong sources of SO_2 (e.g. from industrial sources and at volcanoes) is important as is longer term monitoring at some distance from the source. Furthermore, SO_2 clouds from volcanoes will react with water, in the atmosphere to produce sulphuric acid which can damage aircraft. Accordingly, it would be desirable to be able to warn aircraft of SO_2 clouds.

Wind-blown dust from desert regions or semiarid lands can be a hazard to aircraft, reduces visibility significantly and can cause eye and throat irritation to humans. Large parts of the habitable earth are prone to dust storms, including northern Africa, the Mediterranean

islands, southern Italy, Spain and France, southwestern USA, central and southern Australia, western parts of South America, central China, Japan and south and north Korea and the central deserts of Asia. The wind-blown dust can also be transported long distances - dust from China has been detected in North America. The dust consists of nearly spherical particles of SiO_2 in concentrations that can limit visibility to a few 10's of metres. Accordingly, wind-blown dust can be a significant hazard to aircraft, vehicles and the like.

Accordingly, it would be desirable to provide an apparatus capable of monitoring at least one and preferably all of these adverse atmospheric conditions.

Summary of Invention

An infrared detection apparatus for detecting an adverse atmospheric condition comprising:

a plurality of filters corresponding to different ones of a plurality of wavelengths and at least including filters which enable the adverse atmospheric condition to be detected;

an infrared array, said infrared array producing signals representative of infrared radiation reaching said array;

radiation control means for controlling the infrared radiation received by the infrared array, the radiation control means including means for changing the filters so that said infrared array can produce wavelength signals representative of infrared radiation from each of said wavelengths corresponding to the adverse atmospheric array, and means for enabling said infrared array to produce calibration signals for each wavelength signal;

calibration means for performing a calibration of each wavelength signal to correct for radiation from the infrared detection apparatus on the basis of at least the

corresponding calibration signal to thereby produce a calibrated wavelength signal representative of radiation from the region of sky; and

output means for producing an output indicative of the presence of the adverse atmospheric condition in the region of sky based on the calibrated wavelength signals.

Preferably the apparatus also includes correction means for correcting the calibrated signals for water vapour absorption and/or viewing angle effects

Preferably, the correction means comprises a pre-computed look-up table (LUT). Typically, the LUT is based on off-line detailed radiative transfer calculations which account for the effects of water vapour absorption and for viewing geometry for each of the preferred filtered infrared wavelengths.

Preferably, the means for enabling said infrared array to produce calibration signals comprises a shutter having infrared emissivity which is high in each of said wavelengths.

Preferably, said radiation control means controls said shutter to shut prior to each wavelength measurement to thereby enable said array to produce a calibration measurement corresponding to the preceding wavelength measurement.

Preferably, the calibration means also calibrates on the basis of a pre-calibration.

Preferably, the calibration is performed on the basis of a calibration equation of the form $R = a \times C + b$, where R is the calibration wavelength signal, C is the wavelength signal, and a and b are coefficients.

Preferably, the calibration means alters the coefficient of the calibration equation on the basis of the calibration signal.

Typically, calibration coefficients are calculated for each filter and for each pixel of the infrared array.

Preferably, said output means outputs temperature difference images derived from at least two wavelengths.

In one embodiment said output means produces an alarm if the adverse atmospheric condition is present.

Preferably, said alarm is produced if the temperature differences exceeds a predetermined value.

The algorithm for enabling the output means is dependent on the atmospheric condition. We have determined algorithms suitable for a number of atmospheric conditions.

Where the atmospheric condition is sulphur dioxide, the algorithm is based on the temperatures $T_{8.6}$, $T_{10.0}$, $T_{11.0}$ and $T_{12.0}$ at four wavelengths, 8.6 μm, 10.0 μm, 11.0 μm and 12.0 μm.

Preferably said algorithm involves determining a first temperature difference $\delta T_1 = T_{8.6} - T_{10.0}$, a second temperature difference $\delta T_2 = T_{11.0} - T_{12.0}$, adding the differences δT_1, δT_2 to obtain a third temperature difference δT_3 used as the basis to determine whether SO_2 is present.

Where said atmospheric condition is volcanic ash, it is preferred that said algorithm is based on a temperature difference between two wavelengths, $T_{11.0}$ and $T_{12.0}$.

Preferably an alarm for volcanic ash is activated if $\delta T_{va} = T_{11} - T_{12} > \Delta T_E$, where ΔT is a temperature threshold.

Preferably, where the atmospheric condition is wind-blown dust the algorithm is $\delta T_{dust} = aT_{8.6} + bT_{11} + cT_{12}$ where a, b and c are constants.

Brief Description of the Drawings

A preferred embodiment of the invention will now be described with reference to the accompanying drawings in which:

Figure 1 is a schematic diagram which shows the camera portion of the apparatus of the embodiments;

Figure 2 shows the filter functions of the apparatus;

Figure 3 shows the variation of elevation angle with temperature difference;

Figures 4a and 4b show variation of elevation angle with temperature difference for two different channel differences;

Figure 5 shows the apparatus of the invention viewing a sulphur dioxide plume;

Figure 6 shows an image produced of SO_2 plume using the apparatus of the present invention;

Figure 7 shows a view of a plume of SO_2 with an explosion;

Figure 8 shows an image of an explosion produced using an ash algorithm;

Figure 9 shows a different image for ash and sulphur dioxide free skies;

Figure 10 is a temperature histogram for the image of Figure 9;

Figure 11 illustrates the Gaussian and thresholding technique for setting an ash alarm;

Figures 12a and 12b show a raw and a calibrated image respectively, illustrating the dramatic effect calibration has on the identification of features;

Figure 13 is a map of test sites;

Figure 14 shows the proximity of Tavurvur volcano to the airport;

Figure 15 has ash and visible images taken from Rababa;

Figure 16 shows the alarm histogram for Figure 15;

Figure 17 has ash and visible images from Matupit;

Figure 18 shows the alarm histogram for Figure 17;

Figure 19 is a view of an eruption from Rabaul Volcanological Observatory;

Figure 20 is a graph of an alarm time-series;

Figure 21 has ash and visible images from Hamamas Hotel; and

Figure 22 shows the alarm histogram for Figure 22.

Description of the Preferred Embodiment

The preferred embodiment provides a detection apparatus for monitoring infrared signals from a region of sky in order to detect an adverse atmospheric condition such as volcanic ash, sulphur dioxide or wind-blown dust.

The infrared detection apparatus consists generally of a camera portion 1 as shown in Figure 1 and a processing means such as a computer (not shown) which processes the signals output of the camera 1.

The camera 1 itself comprises a filter wheel housing 2 which optionally has a Germanium window 3, a shutter 4, a filter wheel cover 6 and a filter wheel. Infrared array housing 8 contains an infrared array 9 and a signal processing unit 10.

Output from the signal processing unit is on signal lines 11a which have an Ethernet interface to the computer (not shown) which can process the signals. Lines 11b allow the shutter control signals to be received and also temperature measurements passed to the computer. The temperature measurement corresponds to the temperature of

the shutter 4 and is obtained by a contact thermometer (not shown).

The infrared detection apparatus operates by infrared signals from the region of sky being monitored above at up to five pre-defined wavelengths. The wavelengths which are used depend on the adverse atmospheric condition which is being monitored. The central wavelengths and wavelength intervals are given in Table 1. Herein the term "wavelength" is used to refer to a band of wavelengths. The infrared radiation measured by the detector 1 is linearly proportional to the resistance change in the detector, which is recorded and logged by the signal processing unit. In the preferred embodiment the infrared array is an uncooled microBolometer staring array of 320 x 240 elements sensitive to radiation in the 6-14 μm wavelength interval is used to detect filtered radiation. The detection apparatus uses a filter wheel to filter radiation. The radiation from the sky is focussed onto the array by means of focussing optics in the form of lens 5 and the field-of-view is a cone of up to 90 degrees.

As indicated above, in the preferred embodiment, the infrared array will be an uncooled microBolometer array of dimensions at least 320 x 240 elements, but 640 x 480 elements is also possible. There is a trade-off between the number of elements, cost and maximum spatial resolution per pixel for a fixed optical arrangement. The microBolometer operates on the principle that a temperature change produced by radiation falling on the detector produces a linear resistance change in the material. There are three types of bolometer in commercial use: metal, semi-conductor and super-conductor. In the preferred embodiment either VOx and Si-based semi-conductor bolometers can be used as these are available commercially. However, it would be possible to use a

cooled array with a cryogenic cooler with the ground-based device if the performance criteria cannot be met with an uncooled array.

The infrared detection apparatus can be used to obtain measurements at up to five separate wavelengths to be filtered and also can have a single broadband channel depending on what atmospheric condition is being monitored. The apparatus uses a filter wheel mounted with circular interference filters. Table 1 provides the information for the selection of the filters.

The filters will be 50 mm diameter germanium/ZnSe multi-layer interference filters mounted on a rotating wheel and driven by a stepper-motor. (But, smaller or larger diameter filters may be used depending on the field-of-view required and the focusing power of the optics). Thus, the filter wheel provides point of a radiation control means for controlling the infrared radiation received by the infrared array 9.

The array 9 has a nominal noise temperature of no less than ≈50 mK in the broadband channel. To achieve sufficient temperature sensitivity in the narrow band channels, frame averaging is employed. Table 1 shows the theoretical noise equivalent temperatures (NEΔT's) expected for various frame averaging values in 5 narrow wavelength bands or channels and one broadband channel 20. Thus five narrow band channels centered around 7.3 μm, 10.1 μm, 11 μm and 12 μm are shown in Figure 2 as items 21, 22, 23, 24 and 25 respectively.

Band	High	Low	NEΔT	4	8	16	32	64
7.3	7.05	7.55	1346	673	476	337	238	168
8.6	8.35	8.85	890	445	315	223	157	111
10.1	9.85	10.35	643	322	227	161	114	80
11	10.75	11.25	657	329	232	164	116	82
12	11.75	12.25	900	450	318	225	159	113
8-14	8	14	65	33	23	16	11	8

Table 1: Noise equivalent temperatures (NEΔT, mK) for different amounts of frame averaging.

Table 1 shows noise equivalent temperatures over 1, 4, 8, 16, 32 and 64 frames. It will be seen that for each doubling in the number of frames the noise equivalent temperature is reduced by approximately 30%.

In order to produce an output indicative of the presence of an adverse atmospheric condition, it is necessary to calibrate or correct the raw data produced by the infrared array.

The apparatus of the preferred embodiment is calibrated so that the processing means can produce corrected radiance values which then can be used to produce scene temperatures which can subsequently be processed using an algorithm specific to the atmospheric condition in order to determine the presence of the adverse atmospheric conditions. The calibration process consists of a pre-calibration and a field calibration. The calibrations correct for radiation from the infrared detection apparatus. In particular the field calibration is required in order to correct for changes in the radiation from the infrared detection apparatus during operation. Thus, the field calibration technique is a key feature which allows sufficiently accurate determination of the presence (or not) of the adverse atmospheric conditions.

Figure 12a shows a typical scene where the image is constructed from the raw signals, without calibration. Figure 12b shows the same scene this time after calibration and conversion to temperature units. Aspects of the scene not visible in the raw data are now clearly noticeable in the calibrated data.

The camera 1 provides raw digital counts as output detector array 9 that have also had some corrections applied. These counts can be related to the scene radiance through a linear calibration process, and then to temperature through use of the Planck function.

A two point blackbody pre-calibration procedure was developed which uses the output from the detector array 9 corresponding to two cooled and heated blackbody cavities placed in front of the lens. The calibration equations are:

$$R_{i,c} = a_i C_{i,c} + b_i, \qquad (1)$$

$$R_{i,h} = a_i C_{i,h} + b_i, \qquad (2)$$

where, the subscripts c and h to the cold and hot blackbodies, and i refers to the channel or filter number being used, R = radiance, C = counts and a and b are coefficients corresponding to a gain and an offset respectively. In practice the camera views over a band of wavelengths and the response of the camera (detector and filter) as a function of wavelength must be known. The radiance is therefore related to the scene temperature, T_s, through,

$$R_i = \int_{\lambda_1}^{\lambda_2} B[\lambda, T_s] F(\lambda) d\lambda, \qquad (3)$$

where λ is wavelength, F is the response of the system, and B is the Planck function.

To convert from the calibrated radiances to scene temperature, (3) must be inverted. This is a non-linear problem which requires a minimisation procedure. The approach adopted is to generate a series of look-up tables that give radiances equivalent to a series of pre-specified temperatures. Once the measured radiance is known by combining (1) and (2), the look-up table is searched and interpolated (if necessary) to determine the closest scene temperature. The procedure is accurate to 10 mK over the range of observable temperatures 220 K to 330 K.

The procedure to pre-calibrate the camera 1 is:

- the camera is allowed to acclimatise to the environment for a period of several minutes - this ensures that the camera lens is neither heating up nor cooling down,
- the filter wheel is commanded to move the appropriate filter into position,
- the cold blackbody is moved in front of the lens,
- several frames (up to 24 in the current configuration) are acquired, averaged and stored on the camera memory,
- the hot blackbody is moved into view (in front of the lens),
- several frames (up to 24 in the current configuration) are acquired, averaged and stored on the camera memory,
- the process is repeated for the next filter,
- after completing all required filters the camera is commanded to send the data across a communications line to a computer.

A separate set of calibration coefficients a_i, b_i is developed for each pixel within the 320 x 240 image. Towards the edges of the image the quality of the calibration degrades due to image distortions and non-uniformity of the blackbodies. The blackbody temperature is measured in one place on each blackbody and non-uniformity of the temperature field will occur to some degree.

The pre-calibration procedure is repeated several times and average look-up tables are generated. Typically the pre-calibration is performed in the laboratory and not done in the field. This is possible because we have developed a field calibration technique for altering the coefficients to account for the optics (particularly the lens) that may be heating up or cooling down and thus be at a different temperature to its value when calibrated in the laboratory. This causes an off-set in the measured signals. Our innovative field calibration procedure makes use of a single shutter measurement just before measurements are taken at each wavelength. The shutter fills or slightly overfills the field of view of the instrument and provides a uniform radiation source to the detector. The temperature of the side of the shutter facing the lens is continuously monitored using a contact temperature probe. The shutter side facing the lens is blackened so that its infrared emissivity is high (exceeding 0.98) and uniform across the region 6-114 μm. In the field, the calibration is performed by making a single measurement of the shutter, followed by a measurement of the scene and then application of the calibration equations and shutter measurement which accounts for the off-set generated by any change in temperature of the lens or other radiating surfaces in front of the detector.

The calibration means also calibrates for background atmospheric conditions and viewing angle. That is, the temperature differences on a single channel will vary depending on the channel measured.

In clear and cloudy skies when there is no ash or SO_2 present, water vapour causes differential absorption of radiation in the atmospheric window between 6-14 μm. Thus when comparing two channels there will be a temperature difference. Theoretical calculations and modelling studies indicate that this difference will be negative when the camera views the sky above the horizon. The exact value of the difference depends on the amount of water vapour, but also on the path length that the radiation traverses through the atmosphere. Figure 3 shows the theoretical variation of the temperature difference (11-12 μm) with elevation for a cloudless atmosphere containing about 3 cm of precipitable water. At low elevation angles the temperature difference is slightly negative, but gets progressively more negative until at around 60 degrees elevation when the difference decreases slowly. A consequence of this behaviour is that it is not possible to set a constant threshold for deciding whether infrared difference images contain ash affected pixels. Figure 4a shows the difference as determined from measurements made at Saipan. The variation with elevation angle mimics the theoretical behaviour. The same effect with elevation can be seen for 8.6-12 μm temperature differences (Fig. 4b), except that after 60 degrees the difference starts to increase rather than decrease. This is not seen in the modelling results, and more data are required to determine the cause of this effect. These data show more variation than the theoretical studies because the scene also contains clouds and unmodelled water vapour variations. Nevertheless, the temperature difference decreases with elevation angle in

al cases studied and agrees with the theoretical behaviour.

When the variations and temperature difference are understood, temperature difference can be corrected for inorder to correct the output images so that the output temperature difference images correctly reflect the presence of the adverse atmospheric condition being detected.

The algorithms and temperature differences which are used will depend on the adverse atmospheric condition which is being detected.

SO_2 Algorithm

Figure 5 shows a digital image of the camera viewing towards the Etna volcano in the background with a plume of SO_2 30 emitted from the crater. An SO_2 image produced by the apparatus within 30 minutes of the digital image is shown in Figure 6. The colour scale 22 is drawn to indicate the amount of SO_2 in the plume - from yellow, indicating low amount, to brown, indicating high amounts.

The background to the images comprises light areas of blue and green indicating a colder background whereas the bottom of the image which is dark in colour represents the ground. These areas are labelled 33 and 34 respectively. The left vertical axis represents elevation in degrees and the horizontal axis represents Azimuth. The images are typically produced in colour as indicated above however it will be appreciated that appropriate grey scale images can also be produced. The colour images make iteasy to discern the plumes from the background.

The actual SO_2 index is based on a 4-channel algorithm, while the image itself utilizes all 5 channels,

the 4 narrow band channels and a wide band channel. The SO_2 index is derived by:

(1) forming the difference between a channel centred at 8.6 μm and a channel centred at 10.0μm, label this difference as δT_1,

(2) forming the difference between a channel at 11.0 μm and a channel centred at 12.0 μm, label this difference as δT_2,

(3) adding differences δT_1 and δT_2, label this δT_3,

(4) subtracting a reference value δT_4, which depends on the viewing elevation of the camera, and has a typical range of 1-3°C, label this δT_4 this is the SO_2 index).

The displayed image is produced by scaling δT_4 and overlaying this scaled image into the broadband image so that all pixels in the δT_4 image with a scaled value in the range 1-32 are preserved and all pixels outside this range are replaced by the broadband image pixels. A suitable colour table is then attached to the image and a reference grid and scale are incorporated.

The resulting image (Figure 6) shows SO_2 plume in yellow to brown colour, water vapour (in various degrees of amount) in grey colours, the background (colder) sky as blue and green and topographic features (mountain, ground, trees etc., which are generally warmer than the plume) as dark grey to black.

The SO_2 index derived in this way is linearly related to the temperature difference. In reality there is a nonlinear relation between the temperature differences and the SO_2 amount measured in atm cm or other suitable units. This relation is of the form:

$$u = ln[\alpha\delta T_4 + \beta],$$

where α and β are parameters that depend on the absorption coefficient of SO_2 around 8.6 μm and on instrumental characteristics. u is the absorber amount in suitable units. The parameters α and β are determined from modelling studies and from calibration data for the instrument, including the response functions of each filter. Suffice to note here that the linear approximation used to derive the SO_2 index is a reasonable approximation to the nonlinear algorithm.

It would also be appreciated that any appropriate graphical representation can be used. However, the use of a colour graded output scale is preferred because this allows continuous monitoring of the atmospheric hazard.

Volcanic Ash Algorithm

A volcanic ash algorithm which can be used with the apparatus may be stated as:

$$\delta T_2 = T_{11} - T_{12} > \Delta T_t,$$

where the subscripts 11 and 12 refer to the channel central wavelengths and ΔT_t is a temperature threshold that depends on the water vapour content of the atmosphere and on the viewing elevation angle of the camera. The nominal value for ΔT_t is 0°C. Data (pixels) with values above the threshold are regarded as volcanic ash. Data (pixels) below the threshold are regarded as not volcanic ash.

In testing, the apparatus was also able to capture discrete explosions from the Stromboli Volcano. An example of this is shown in Figure 7. In the case of the explosion, the pyroclastic material is mostly volcanic hot rocks, cinders and ash and reveals itself as grey to black colours 41 when the SO_2 algorithm is used. An SO_2 plume 42

is clearly shown. In contrast when the ash algorithm is used, that is, by taking temperature differences using two channels, specifically δT_2, the image shown in Figure 7 is obtained. The colour scale now shows positive temperature differences in shades of orange and red, and negative differences as blue to yellow. In this case the algorithm identifies the hot rocks and cinders as positive differences 40 (high ash content), and resuspended ash as slightly negative (similar to the material on the surface of the mountain slopes). The sky has markedly negative differences.

Wind-Blown Dust Algorithm

Desert dust has a high silica (SiO_2) content and when small particles (diameters less than 10 μm) are suspended in the atmosphere they disperse infrared radiation in a similar fashion to volcanic ash particles. Consequently, the algorithm used to identify ash in the atmosphere can also be used to identify wind-blown dust. Dust storms are a frequent and global phenomenon. Most of the dust is confined to the boundary layer - the part of the atmosphere closest to the surface and generally not extending more than 5 km upwards. Occasionally, large dust storms can be transported vast horizontal distances (may 1000's of kilometres) and be lifted to heights greater than 5 km. Dust storms have been identified using passive infrared radiation from satellites. The dust algorithm differs from the ash algorithm in one important aspect. Since it is unlikely that wind-blown dust will contain any appreciable amounts of SO_2 gas (the reverse being true for ash), a channel at 8.6 μm, can be used in conjunction with the 11 and 12 μm channels. The dust algorithm thus uses three channels rather than two. The form of the algorithm is:

$$\delta T_{dust} = aT_{8.6} + bT_{11} + T_{12},$$

where the subscripts 8.6, 11 and 12 refer to the central wavelengths (in μm) for each channel and *a*, *b* and *c* are constants. The nominal values of these constants are: *a = 1, b = 1 and c = -1*.

It will be appreciated that it will not always be convenient or appropriate for someone to monitor the image data from the apparatus. Accordingly, an automated algorithm can be developed in order to initiate an alarm. This alarm is based on analysis of the difference images produced in accordance with the algorithms. However, it will be appreciated that the images do not actually have to be produced in order for the alarm to be triggered. An example of an alarm algorithm suitable for volcanic ash is described, however it is be appreciated that other alarm algorithms can be developed.

To minimise operator intervention of the infrared image data and trigger the transmission of an image to the users, an automated algorithm has been developed - i.e. to transmit the image data to users when there is sufficient reason for a user to inspect the image. The algorithm or 'alarm' is based on a histogramming technique that takes into account the viewing elevation and the amount of water vapour in the atmosphere. As there are 320 x 240 image pixels in a single difference image (ΔT_1, ΔT_2, ΔT_3). Due to cloud movement, noise, calibration errors and sensitivity limitations, some pixels will appear anomalous when there is little or no hazard within the image. The histogramming technique accounts for these anomalies.

In general the structure of these anomalies is very different to that expected from an ash cloud. However, on a pixel-by-pixel basis it is impossible to determine whether the signal is due to a camera anomaly or due to a real ash signature. Analysis of the images obtained from

Anatahan in conditions where ash was known to be present suggests that the use of structure in the images can be used to set a threshold or alarm to indicate the presence of ash. To demonstrate how this can be done we first consider a set of images obtained in conditions where there was no ash or SO_2. Figure 9 shows an image obtained in ash/SO_2-free conditions viewing with an elevation of 20 degrees above the horizon. The colour scale on this image indicates a temperature range from -15 K to +10 K, with red-coloured pixels having the most positive temperature difference. To highlight the region where most ambiguity might exist, a grey-scale showing temperatures from -0.5 K to +0.5 K is included within the main colour scale. Thus grey-coloured pixels in the temperature difference image may be regarded as *marginal*, in terms of detectability. In this image there are some grey-coloured pixels, but the majority of the pixels are yellow, green to blue indicating negative temperature differences and hence normal conditions (i.e. clear skies or water/ice meteorological clouds). The 2-dimensional histogram of this image is shown in Figure 10. The same temperature range and colour scale are used for the histogram. From theoretical and modelling calculations we expect pixels that are ash contaminated to have positive differences. But, their actual value depends on viewing conditions, particularly the viewing elevation, and also the amount of water vapour in the path. Accordingly, we have determined that a threshold value of 0 K for ash is appropriate under most conditions. The image shown above was obtained at 20 degrees elevation and as the field-of-view of the infrared camera is roughly 24 degrees in the vertical direction, some parts of the image view land surfaces. The histogram has prominent peaks at roughly -1 K 51 and -5 K 50 which correspond to clouds and clear skies, respectively. In this case the least negative peak has a tail that includes some positive pixels. In the corresponding image these pixels correspond to viewing features that are low on the

horizon and include ground targets. Such 'anomalies' are difficult to isolate in an automated manner and could give rise to *false alarms* if a straightforward pixel thresholding technique were employed.

The scheme chosen to automatically determine whether an image has detected ash is a statistically based method. This is the method of choice because by the nature of the problem there is often going to be a distribution of pixels that can be flagged as ash, within an image that has many pixels that are definitely ash or definitely not ash. In addition, because of the likelihood that pixels will contain mixtures, a simple threshold and binary decision process would be inappropriate.

The histogram shown in Figure 10 consists of two prominent peaks with a spread of pixels around these peaks. If the detection apparatus viewed a target of constant temperature (e.g. a uniform cloud or the clear sky), then simply because of the fact that the camera has a wide field-of-view and there is water vapour absorption along the differing paths to the target, the resulting difference image would be non-uniform. In practice it is unlikely that the sky would present a uniform target and even less likely that a cloud would by perfectly uniform. The combination of these effects leads to a natural spread in the histogram of the temperature differences, with a central peak corresponding to the mode temperature difference. For a relatively uniform scene the peak would be high and the spread (or standard deviation of the distribution) would be low. A natural choice to model this kind of distribution is the normal distribution or Gaussian distribution. The Gaussian distribution in the mathematical terms is,

$$G(\Delta T) = A_0 \exp\left\{\frac{(\Delta T - \mu_{\Delta T})^2}{\sigma^2 \Delta T^2}\right\},$$

where ΔT is the temperature difference, $\mu_{\Delta T}$ is the mean temperature difference, $\sigma_{\Delta T}$ is the standard deviation, and A_0 is the maximum frequency, which occurs when $\Delta T=\mu_{\Delta T}$. Each of the peaks ($i = 1 \ldots n$) within the frequency distribution (histogram plot) is assumed to be centred at $\mu_{\Delta T,i}$ with a spread of $\sigma_{\Delta T,i}$. A set of Gaussian distribution is fitted to the frequency distribution data and the parameters, $A_{0,i}$, $\mu_{\Delta T,i}$, and $\sigma_{\Delta T,i}$ derived. The linear combination of these distributions is the model-fit to the data.

The fit for the histogram data shown in Figure 10 is shown in Figure 11. Three Gaussians were used in the fit:

Parameter	i=1	i=2	i=3
$A_{0,i}$	74.2%	24.9%	0.9%
$\mu_{\Delta T,i}$	-4.24 K	-0.84 K	-0.67 K
$\sigma_{\Delta T,i}$	+1.49 K	+0.33 K	+0.08 K

The fit to the distribution although not perfect, it is sufficient for setting the alarm for the image. The alarm technique now proceeds by setting a *threshold Gaussian* with a mean and standard deviation derived from modelling, and comparing this with the *n*-Gaussian data-fit. The region between the pixels bounded by the *threshold Gaussian* mean value, and the overlap region between the two Gaussians (the *threshold* and the data-fit) is calculated. This area (or number of pixels) is subtracted from the number of pixels that exceed the *threshold Gaussian* mean value and lie within the data-fit Gaussian (see Fig. 11).

The ratios,

$$\left(\frac{P_i - P_{o,i}}{P_i}\right)$$

$$R_I = \frac{A_{o,i}}{\sum_{j=1}^{n} A_{o,j}}$$

where $P_{o,i}$ is the number of overlap pixels for Gaussian i, P_i is the number of pixels that exceed the *threshold* mean, and $A_{o,i}$ are the maxima for the Gaussian fits. The purpose of normalising by the maximum us to ensure that more weight is given to distributions that have well-defined and dominant peaks.

It will be appreciated that any number of different statistical techniques can be used in order to determine whether sufficient numbers of the pixels relate to the atmospheric condition being monitored to warrant the generation of alarm.

Experimental Results

During 26-30 November 2003 CSIRO experimentally operated the detection apparatus at the site of an erupting volcano near Rabaul town, in west New Britain, PNG. The volcano, Tavurvur has ash-rich explosions every 10-30 minutes, with plumes that extend several hundred meters above the crater, approximately 400 m above sea level. A large number of infrared images were obtained at various distances from the crater and employing a variety of viewing angles. The purpose of this field work was to obtain reliable ash images to prove the concept of ash detection from a ground-based platform using uncooled infrared imaging arrays.

The results indicate that the detection apparatus can image ash plumes and clouds and clearly discern these from meteorological clouds. Results are best at closest proximity to the ash cloud, but good results were obtained at distances greater than 5 km from the active crater. The ash alarm algorithm was also tested in an autonomous

manner overnight from a distance of ~8 km.

Measurement Sites

Figure 13 shows the locations of the measurement sites (six in all) used to image the ash-rich eruptions from Tavurvur. They are listed in Table 2.

Site label	Site name	Distance from crater (km)
A	Hamamas Hotel	3.7
B	Rabaul airport (old)	3.0
C	Rababa ("hot springs")	1.8
D	Matupit village	2.5
E	RVO	8.0
F	CPL Mill	7.4

Table 2. Site labels, names and locations used to make measurements of the ash-rich plumes and clouds from Tavurvur volcano (labeled Tavurvur in Fig. 13).

Tavurvur has been active since a major eruption took place in September 1994 which devastated the town of Rabaul and destroyed the airport. A new airport, Tokua, has been constructed and is located about 20 km southwest of Tavurvur. With the crater still active, flights in and out of Tokua only take place in daylight hours and not at all of the winds move the ash towards the airport runway. Figure 14 shows a digital photograph taken from the runway at Tokua. A plume 60 from Tavurvur is noticeable in the background.

The Rabaul Volcanological Observatory (RVO) operates on a hill overlooking the active crater and at about 8 km distance from it. Economic pressures in PNG have meant that only limited resources are available at RVO for operating geophysical equipment and power failures are also common. The main means of transport throughout PNG is by jet and light aircraft and the economy is highly dependent on air transportation. Thus there is an urgent need to monitor the volcanoes in New Britain (there are many) and throughout PNG.

The apparatus of the preferred embodiment operates off batteries for up to 16 hours and can be deployed in relatively hostile environments, rapidly by a single user. To test the ability of the instrument to distinguish ash from other meteorological clouds, the apparatus was deployed at a variety of locations and in a variety of viewing configurations. The measurements were made in an atmosphere with quite high water vapour amounts and at elevation angles varying from 10° to nearly vertical viewing. On many occasions the atmosphere around the instrument was filled with ash particles, making the atmosphere appear grey and causing irritation to the eyes and lungs.

Results

(a) Rababa

The best results were obtained from Rababa, approximately 1800 m from the crater. Note that there are also water clouds 70 in the image and the high frequency of activity has caused the atmosphere to be heavily laden with ash particles.

Figure 15 shows a typical results obtained from Rababa (c). The ash image (left-panel) correctly identifies the plume 71 and clouds of ash from Tavurvur.

Grey to black coloured regions of the image are identified as having no ash. The mountainside 72 is also identified as ash-this is not surprising since the mountain is covered in ash particles.

The automatic alarm algorithm was used on all images and the alarm generated for the image shown in Fig. 15 is shown in Fig. 16. The alarm being generated because of the difference between the actual histogram 100 and threshold histogram 101. About 43% of the pixels are identified as ash in the image and a clear and unambiguous ash alarm has been triggered.

(b) Matupit village

Good results were alo obtained from Matupit village (D) about 2.5 km from the vent. The measurements from Matupit were made in relatively "wet" conditions and drizzle as well as ash fall were observed here. Results were very similar to those obtained from Rababa. To illustrate the ability of the apparatus to detect ash at high elevation angles, Fig. 17 shows an ash image and corresponding photograph of a dispersing ash cloud 75 viewed from 40° elevation.

In this case 73% of the pixels were identified as ash (see Fig. 18).

(c) RVO

Ash images from RVO (E) were the most difficult to obtain because of the distance from the active vent (~8 km) and because the Observatory is perched on a hill; thus the camera could only view at relatively small elevation angles (~10° or less). The combination of the greater distance and small elevation angles means that a considerable water vapour path is traversed (the water vapour absorption masks the positive temperature differences expected from the ash signal). The frequency

of eruption was so high that the air between the camera and the eruption column was often filled with fine ash particles. This has the effect of making the atmosphere appear grey and also causes large absorption in the infrared. The camera was operated continuously overnight at RVO. An example of the scene viewed by the apparatus from RVO is shown in Figure 19.

Since the apparatus operated through the night, we were able to test the alarm algorithm without actually viewing the image data. Figure 20 shows a time-series of alarms detected by the apparatus from RVO.

The series of triangles and circles 81 represent alternate 5-min sampled data and their similarity gives confidence in the results.

The threshold for the alarm has been arbitrarily set to a value of 10%. In practice this will have to be amended to suit the viewing conditions. The plot suggests that there were continuous ash emissions during the night - in agreement with what was observed during the day. Notice that the highest alarm percentages never exceed 35% or so and this is simply a function of the viewing attitude of the instrument. If the instrument were sited closer to the volcano, then more of the ash would fill the field of view of the instrument and there would be a higher percentage for the alarm. Again this is a feature that need to be considered within the context of the viewing geometry and location of the instrument with respect to the activity.

Because the atmosphere around Rabaul was constantly affected by ash it was difficult to obtain images which showed no ash. Some data were acquired looking away from the vent at meteorological clouds during the daytime which suggests the instrument was working as

expected. Figure 21 shows one of the images. In this image the meteorological cloud is mostly light yellow or blue-green, suggesting no ash. The pixels coloured yellow in the bottom right of the image correspond to very low elevation angles and ground targets that often give temperature differences slightly greater than zero. The corresponding alarm histogram was not triggered by these data (see Fig. 22).

It will be apparent to a person skilled in the art that these and many other variations fall within the scope of the present invention.

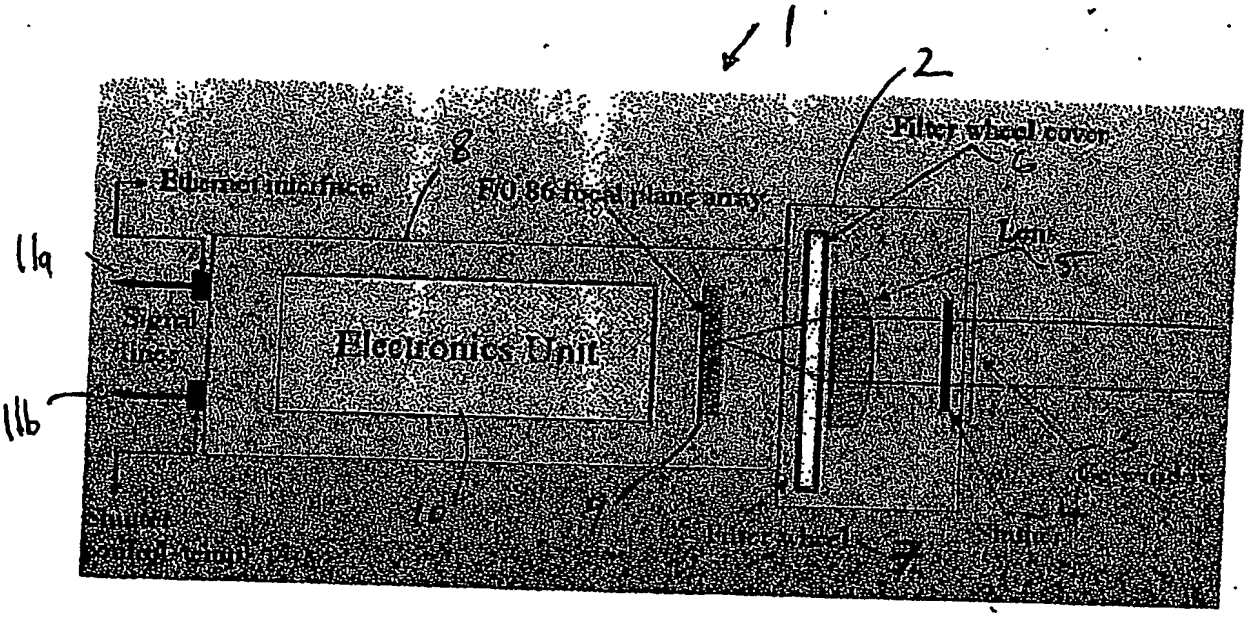

FIGURE 1

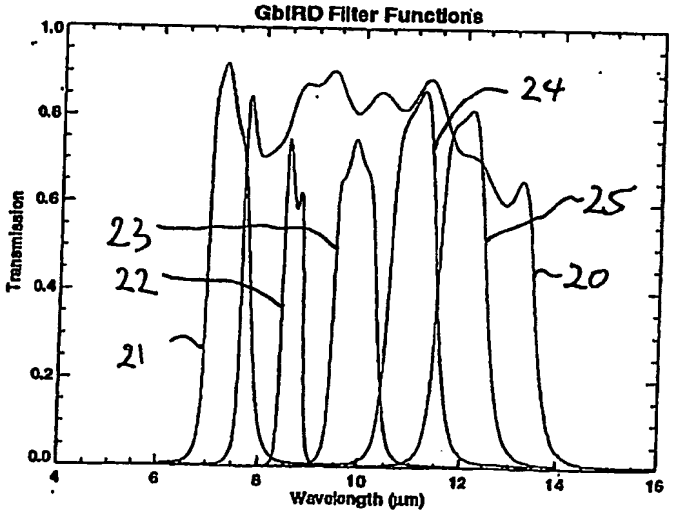

FIGURE 2

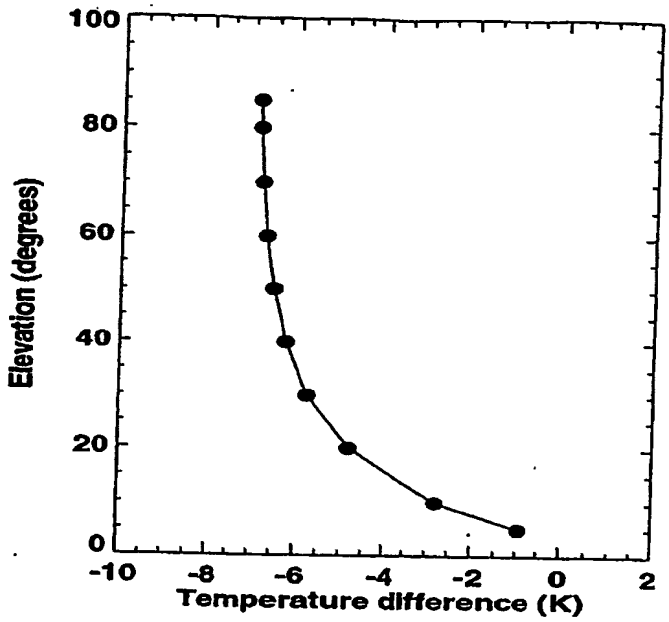

FIGURE 3

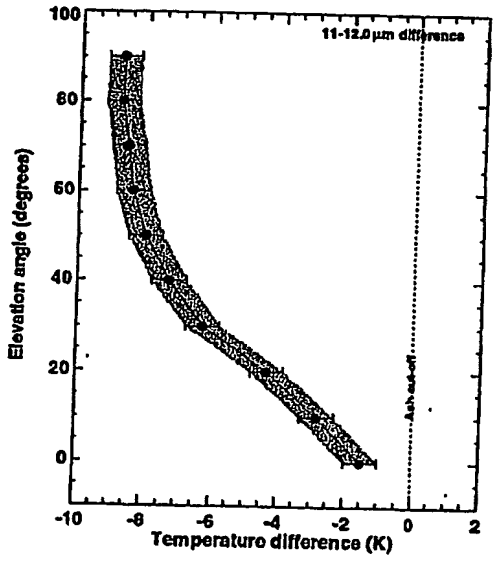

FIGURE 4a

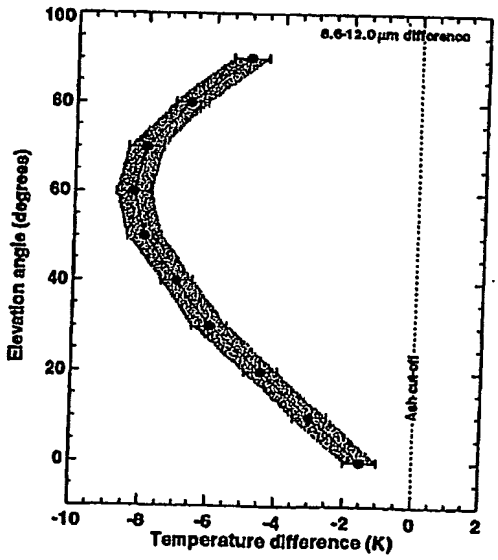

FIGURE 4b

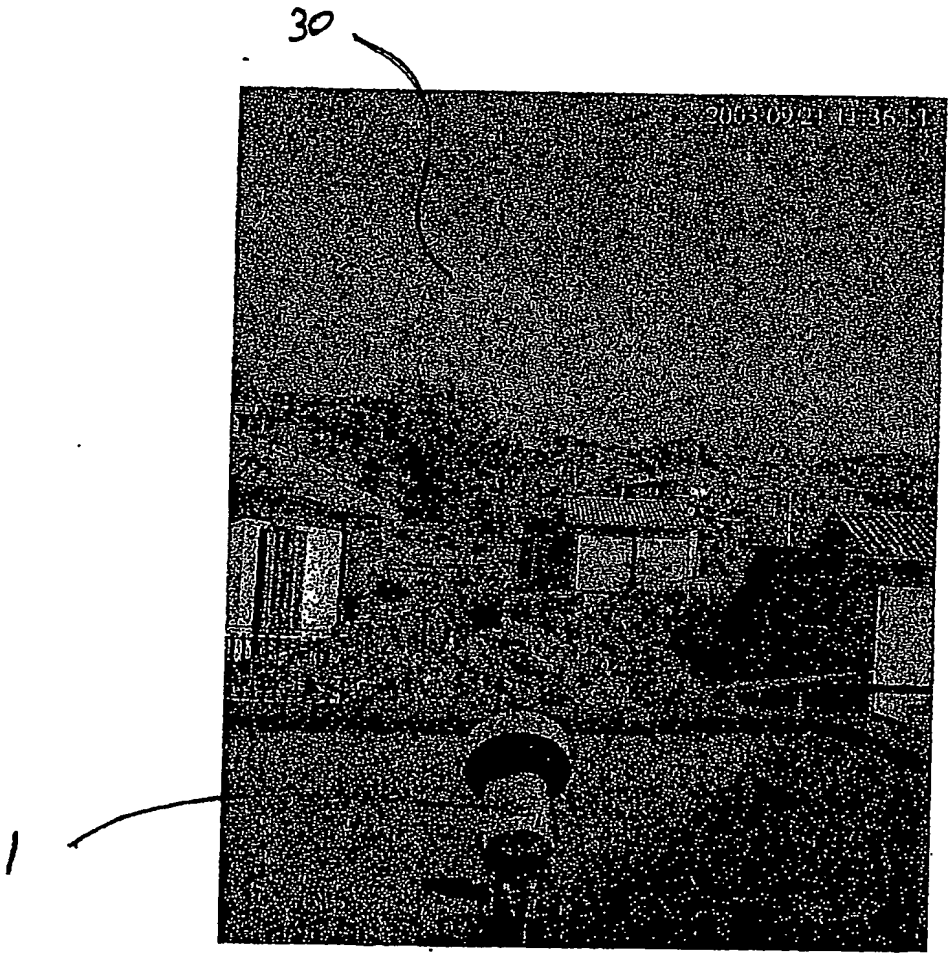

FIGURE 5

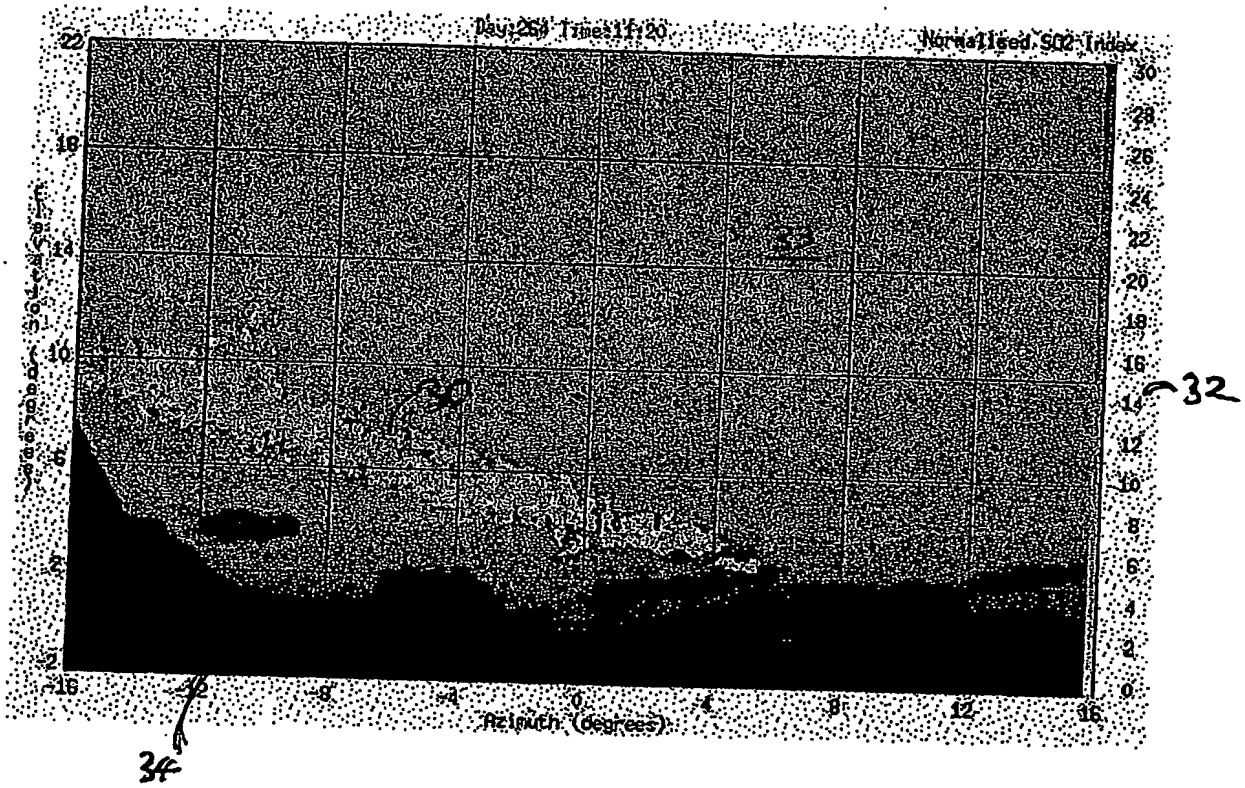
Day: 269 Time: 11:20
Normalised SO2 Index
Elevation (degrees)
Azimuth (degrees)
30
32
34

FIGURE 6

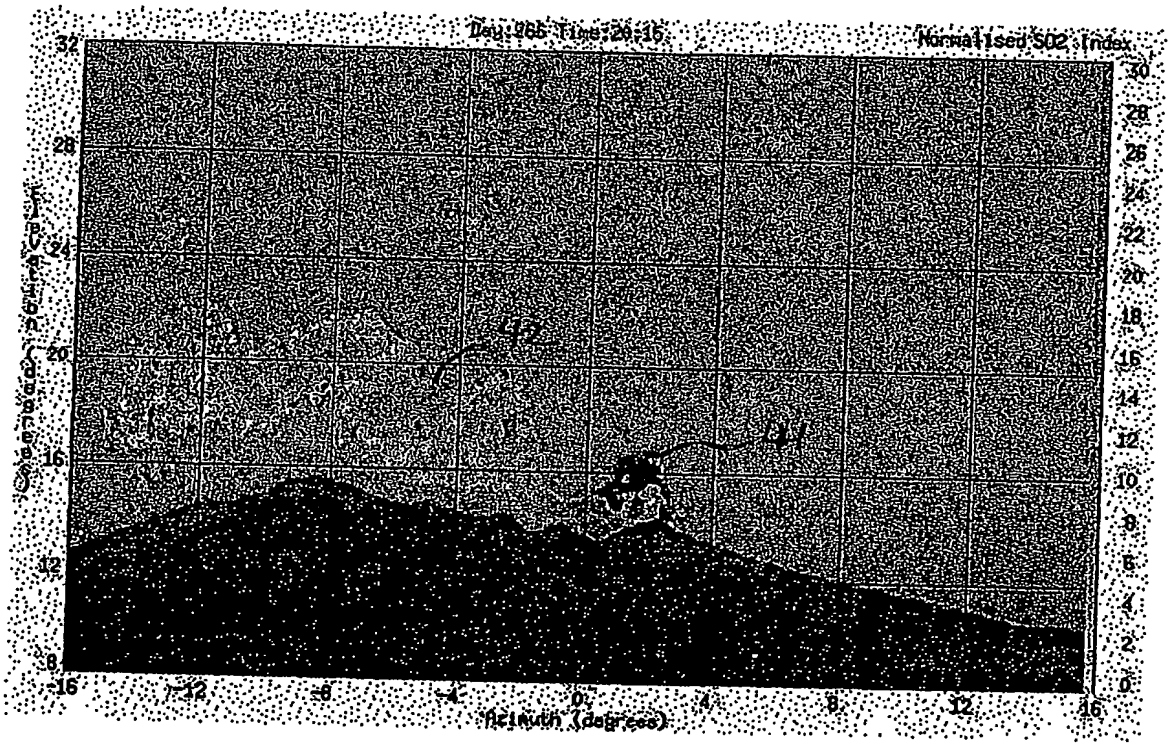
Day:265 Time:20:15
Normalised SO2 Index
Elevation (degrees)
Azimuth (degrees)
32
28
24
20
16
12
8
-16
-12
-8
-4
0
4
8
12
16
30
28
26
24
22
20
18
16
14
12
10
8
6
4
2
0

FIGURE 7

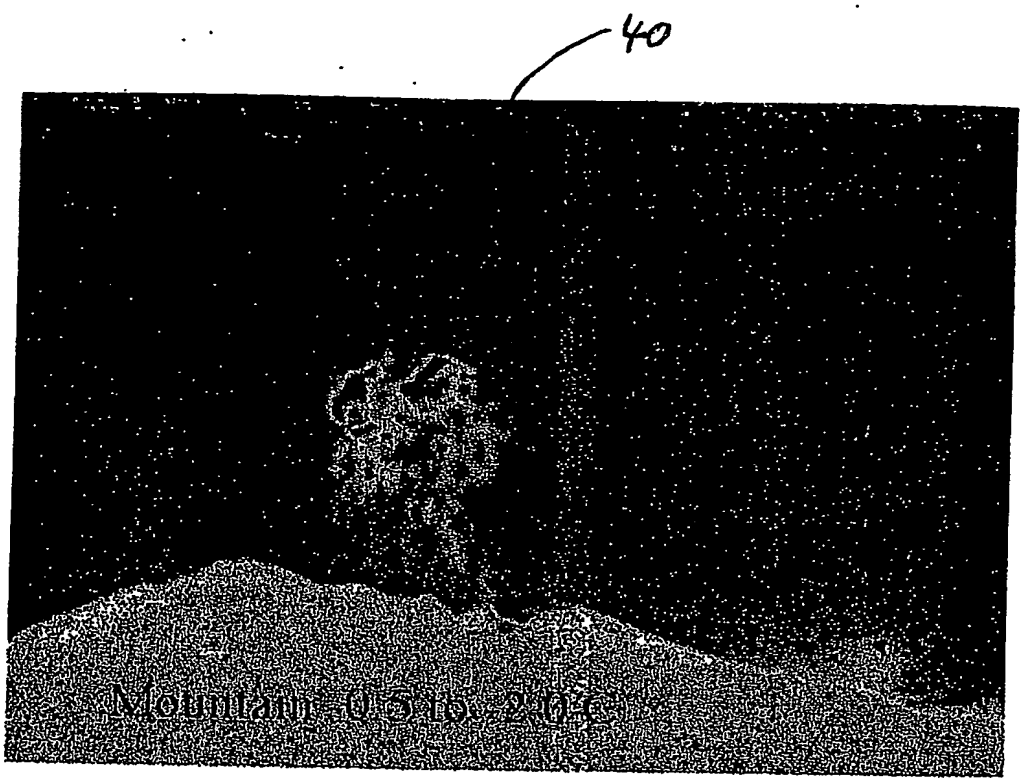

FIGURE 8

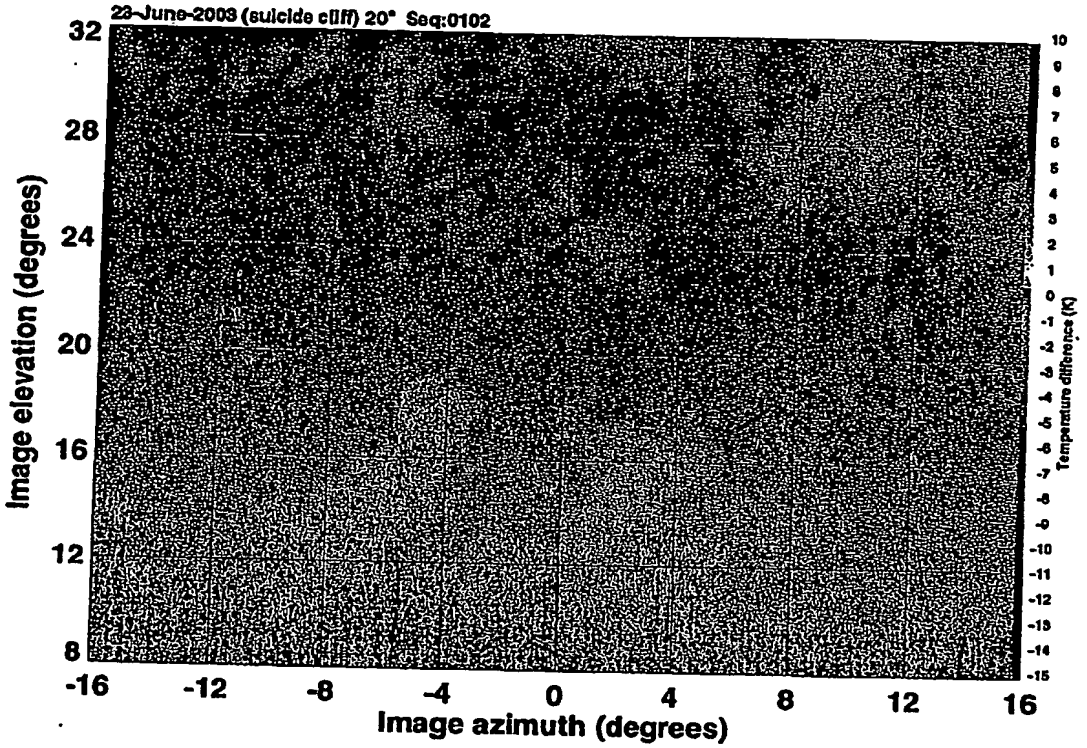
23-June-2003 (suicide cliff) 20° Seq:0102
Image elevation (degrees)
32
28
24
20
16
12
8
-16
-12
-8
-4
0
4
8
12
16
Image azimuth (degrees)
Temperature difference (K)
10
9
8
7
6
5
4
3
2
1
0
-1
-2
-3
-4
-5
-6
-7
-8
-9
-10
-11
-12
-13
-14
-15

FIGURE 9

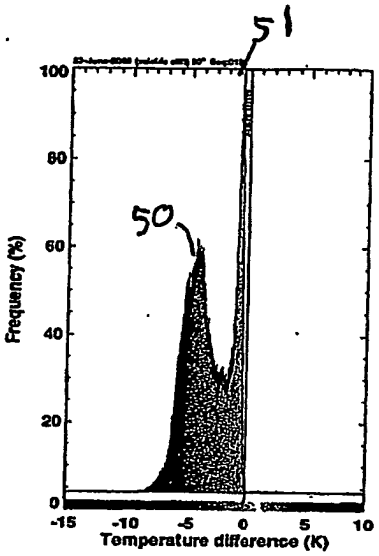

FIGURE 10

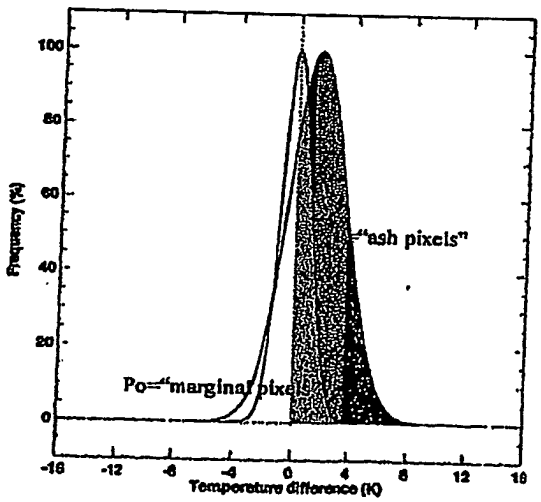

FIGURE 11

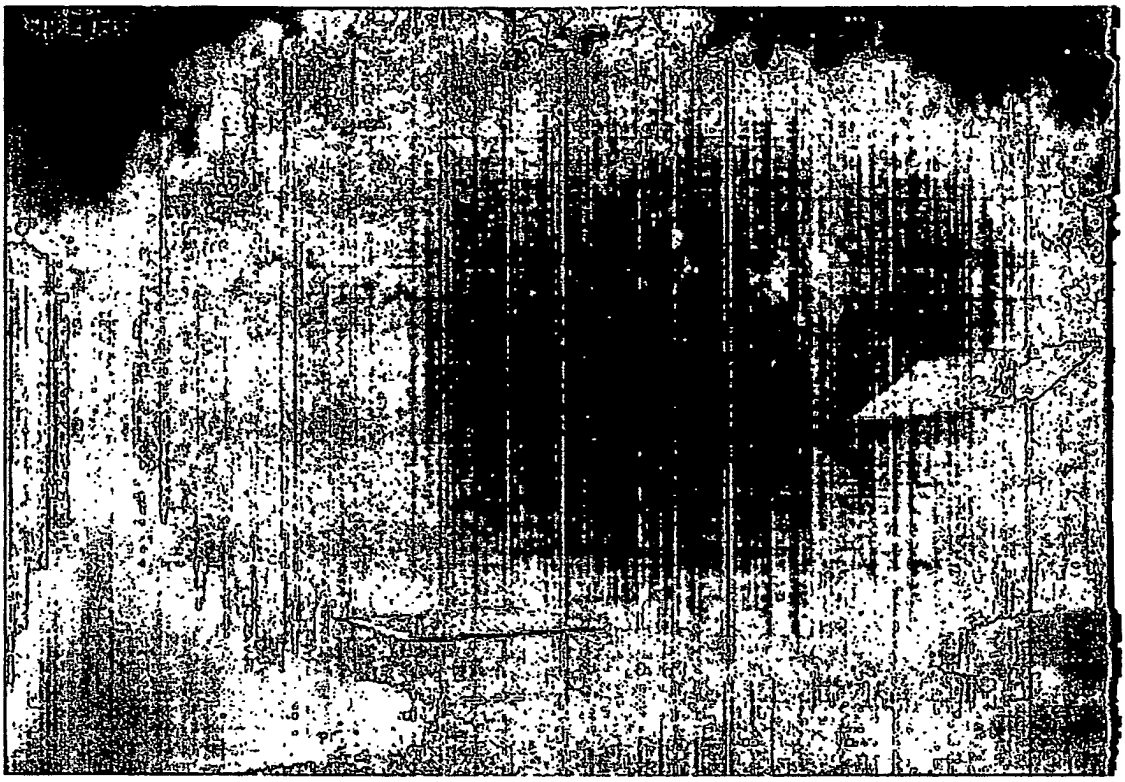

FIGURE 12a

FIGURE 12b

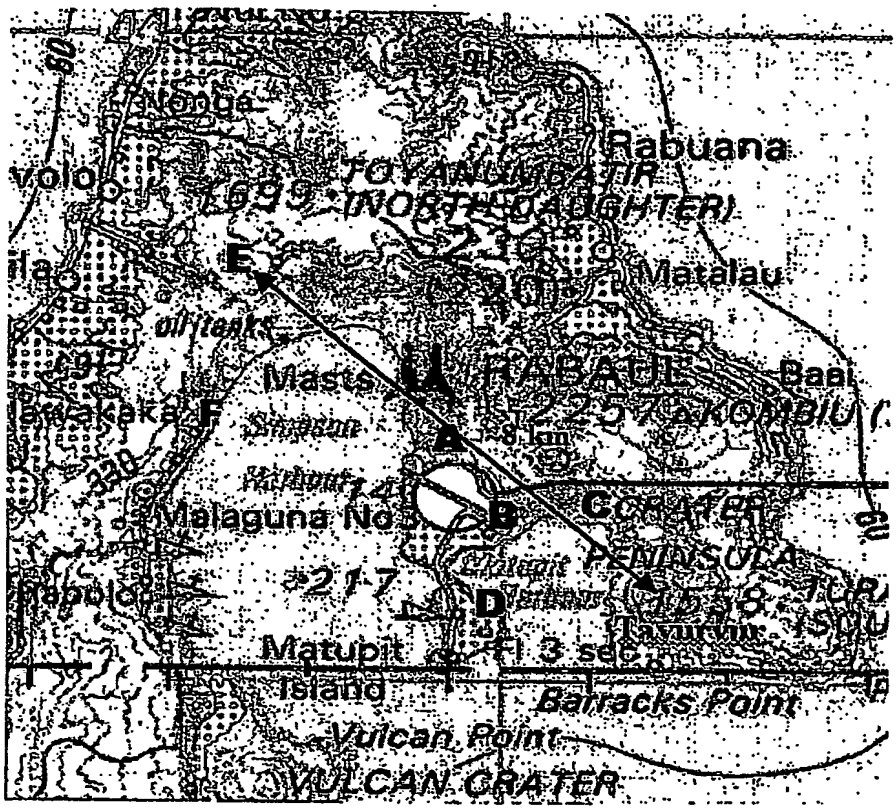
Rabuana
Matalau
Masts
Malaguna No 3
Matupit
Island
Vulcan Point
VULCAN CRATER
Barracks Point
E
A
B
C
D
F

FIGURE 13

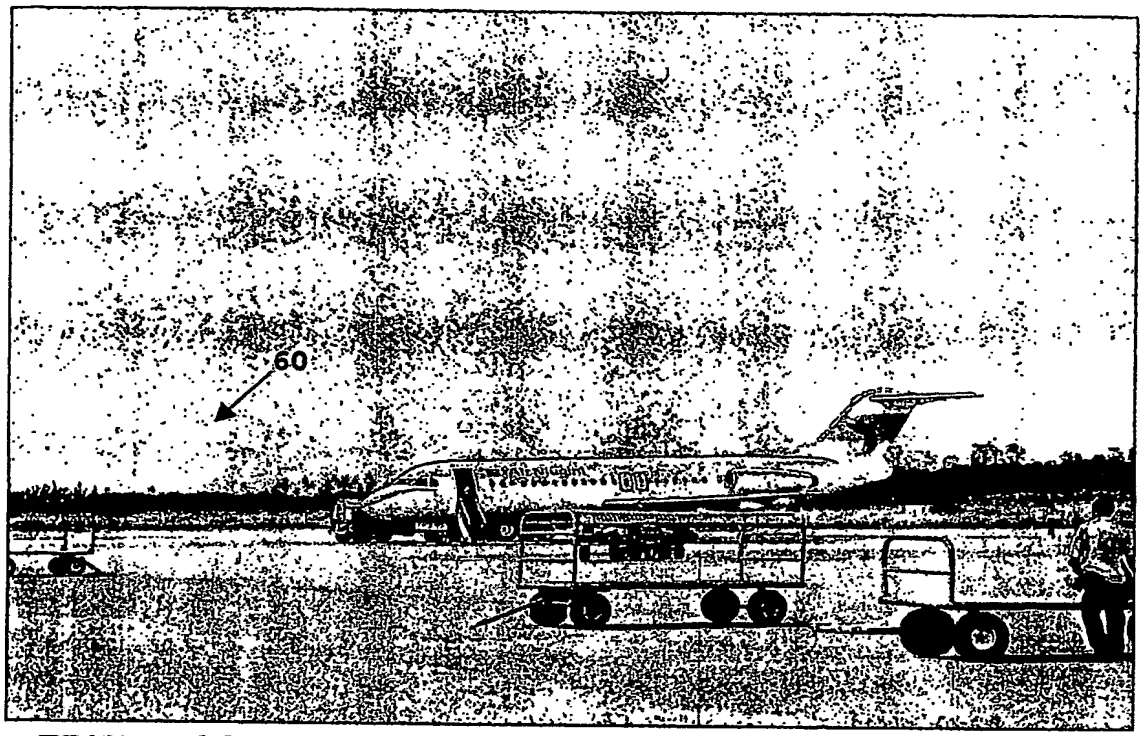

FIGURE 14

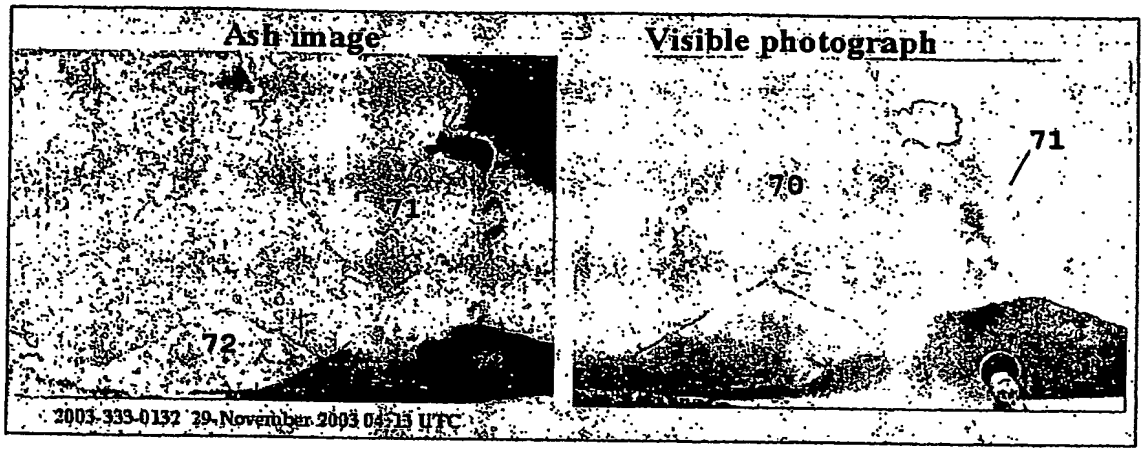
Ash image
Visible photograph
71
72
70
71
2003-333-0132 29-November-2003 04:15 UTC

FIGURE 15

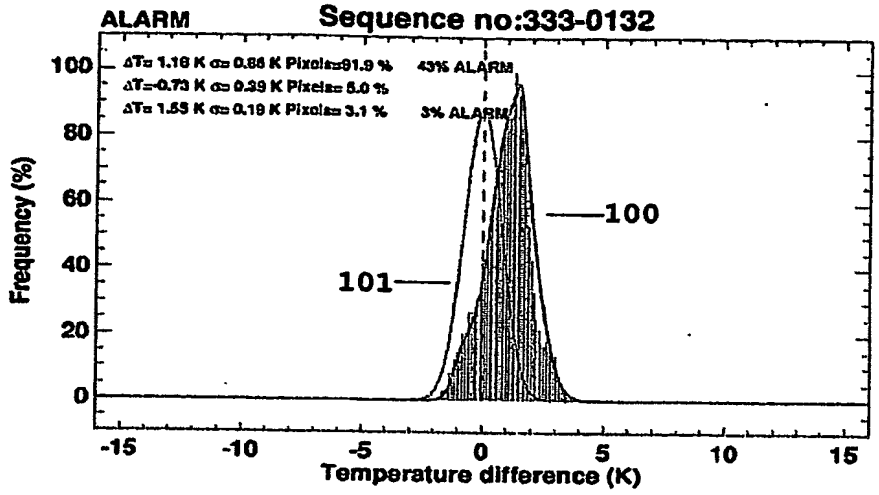

FIGURE 16

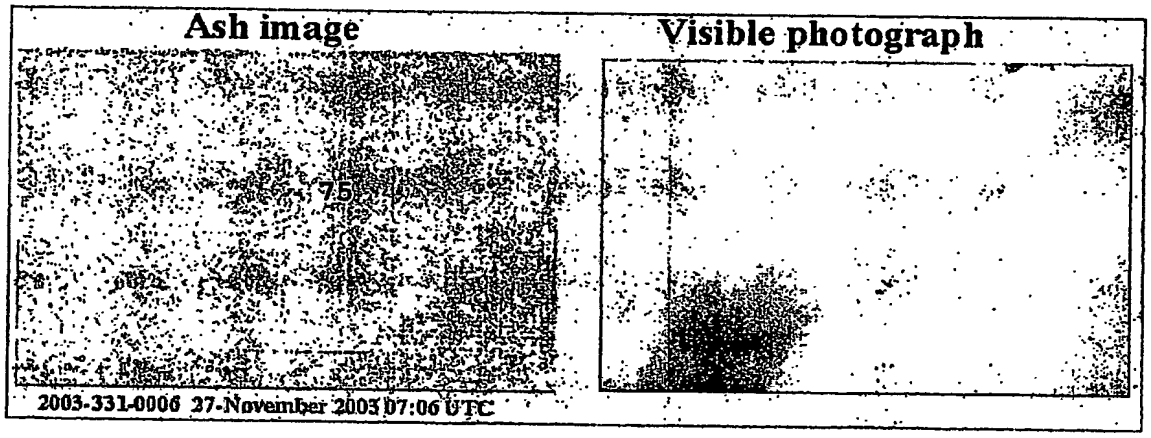

FIGURE 17

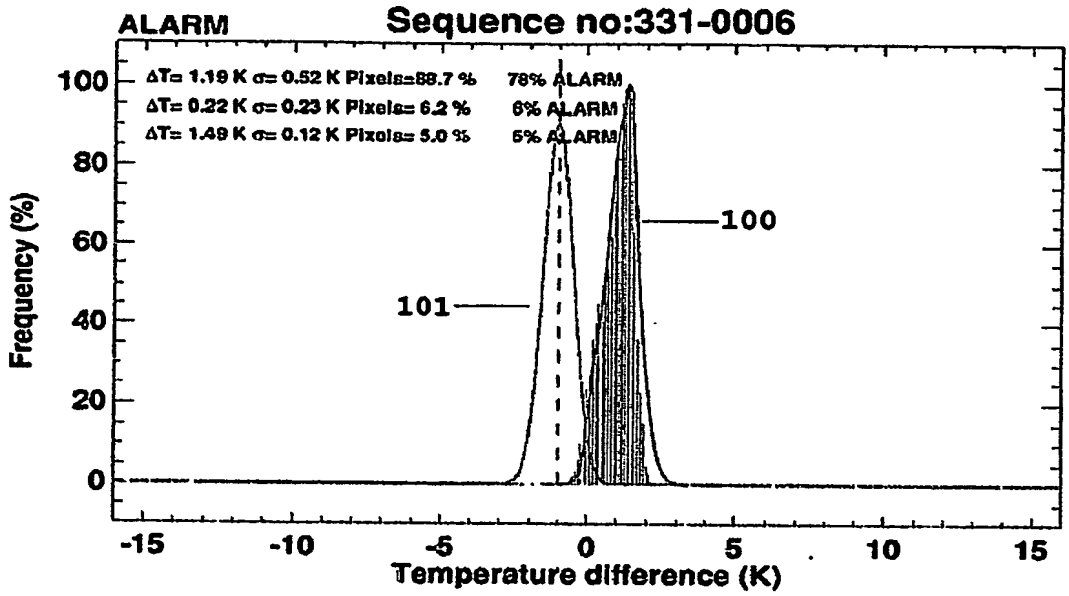
ALARM
Sequence no:331-0006
ΔT= 1.19 K σ= 0.52 K Pixels=88.7 %
ΔT= 0.22 K σ= 0.23 K Pixels= 6.2 %
ΔT= 1.49 K σ= 0.12 K Pixels= 5.0 %
78% ALARM
6% ALARM
5% ALARM
100
101
Frequency (%)
100
80
60
40
20
0
-15
-10
-5
0
5
10
15
Temperature difference (K)

FIGURE 18

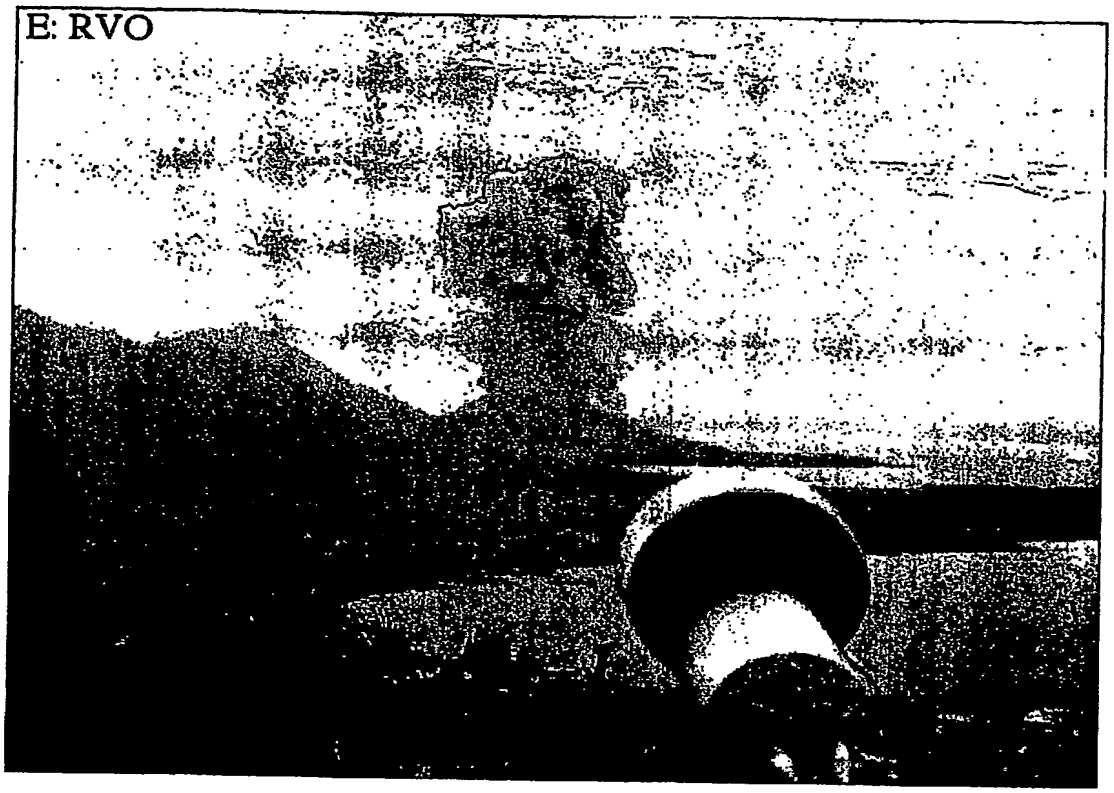

FIGURE 19

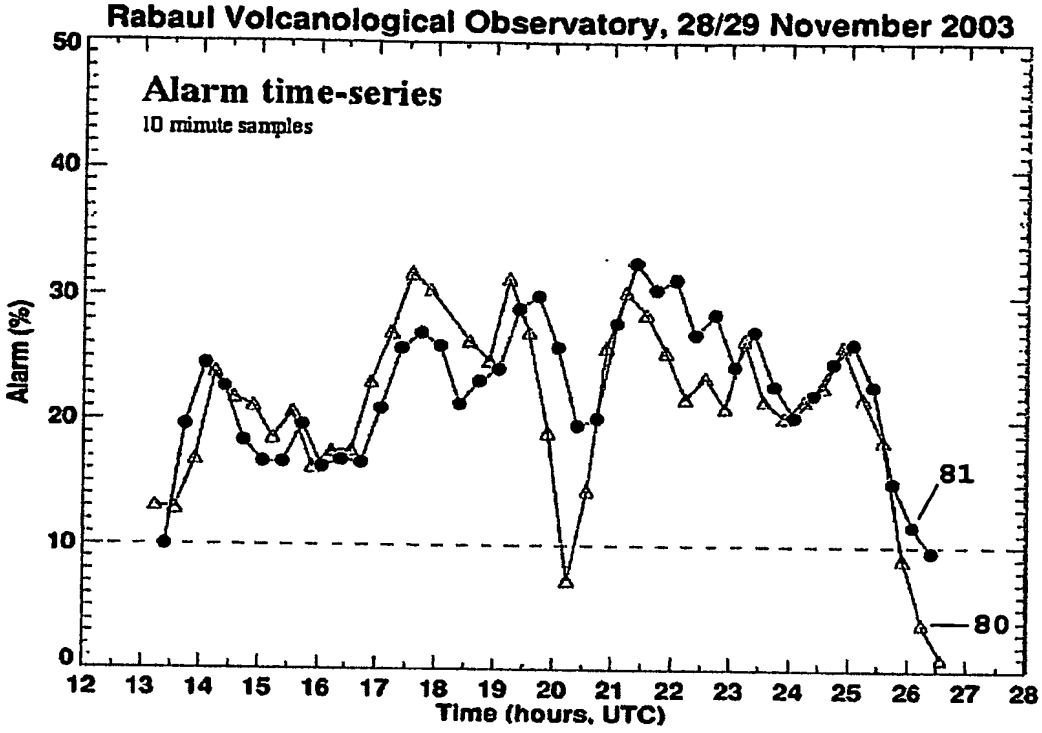
Rabaul Volcanological Observatory, 28/29 November 2003
Alarm time-series
10 minute samples
Alarm (%)
Time (hours, UTC)
81
80
0
10
20
30
40
50
12
13
14
15
16
17
18
19
20
21
22
23
24
25
26
27
28

FIGURE 20

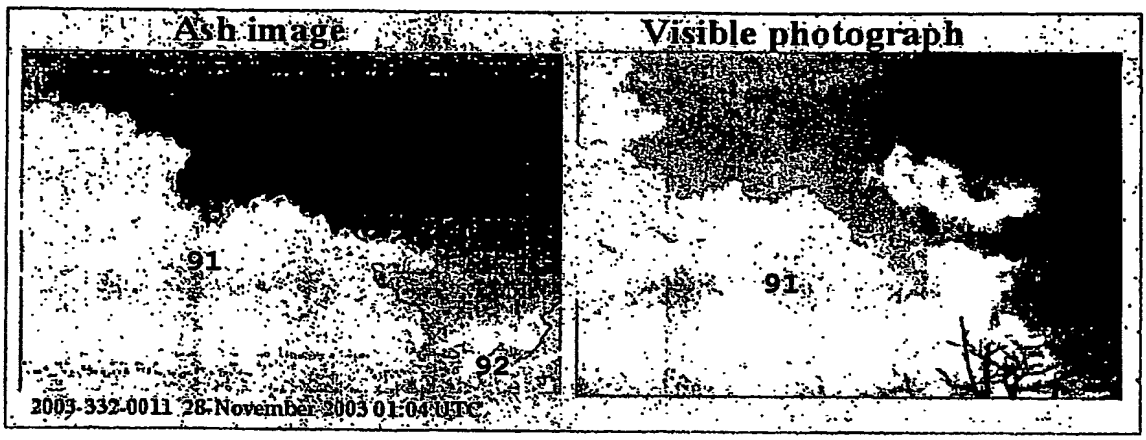
Ash image
Visible photograph
91
92
91
2003-332-0011 28 November 2003 01:04 UTC

FIGURE 21

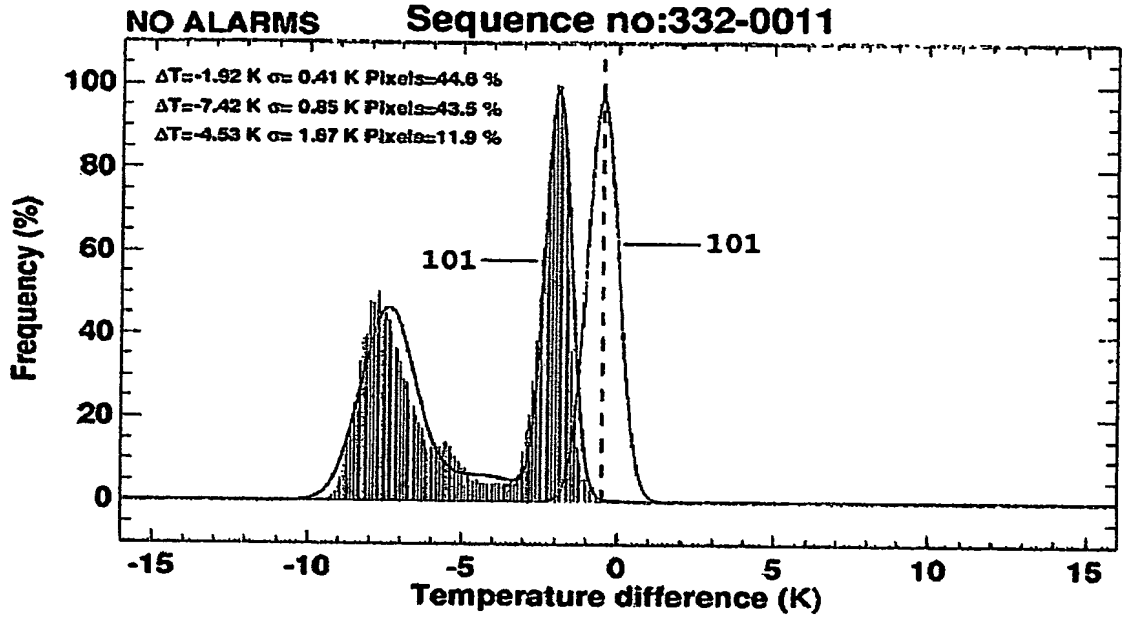
NO ALARMS
Sequence no:332-0011
ΔT=-1.92 K σ= 0.41 K Pixels=44.6 %
ΔT=-7.42 K σ= 0.85 K Pixels=43.5 %
ΔT=-4.53 K σ= 1.67 K Pixels=11.9 %
101
101
Frequency (%)
100
80
60
40
20
0
-15
-10
-5
0
5
10
15
Temperature difference (K)

FIGURE 22

This Page is Inserted by IFW Indexing and Scanning Operations and is not part of the Official Record

BEST AVAILABLE IMAGES

Defective images within this document are accurate representations of the original documents submitted by the applicant.

Defects in the images include but are not limited to the items checked:

- ☐ BLACK BORDERS
- ☐ IMAGE CUT OFF AT TOP, BOTTOM OR SIDES
- ☐ FADED TEXT OR DRAWING
- ☑ BLURRED OR ILLEGIBLE TEXT OR DRAWING
- ☐ SKEWED/SLANTED IMAGES
- ☐ COLOR OR BLACK AND WHITE PHOTOGRAPHS
- ☐ GRAY SCALE DOCUMENTS
- ☑ LINES OR MARKS ON ORIGINAL DOCUMENT
- ☐ REFERENCE(S) OR EXHIBIT(S) SUBMITTED ARE POOR QUALITY
- ☐ OTHER: _____

IMAGES ARE BEST AVAILABLE COPY.

As rescanning these documents will not correct the image problems checked, please do not report these problems to the IFW Image Problem Mailbox.